AD_____

Award Number: DAMD17-03-1-0541

TITLE: Automated Area Beam Equalization Mammography for Improved Imaging of Dense Breast

PRINCIPAL INVESTIGATOR: Sabee Molloi, Ph.D.

CONTRACTING ORGANIZATION: The University of California
Irvine, California 92697-7600

REPORT DATE: August 2004

TYPE OF REPORT: Annual

PREPARED FOR: U.S. Army Medical Research and Materiel Command
Fort Detrick, Maryland 21702-5012

DISTRIBUTION STATEMENT: Approved for Public Release;
Distribution Unlimited

The views, opinions and/or findings contained in this report are those of the author(s) and should not be construed as an official Department of the Army position, policy or decision unless so designated by other documentation.

20050415 212

REPORT DOCUMENTATION PAGE

1. AGENCY USE ONLY (Leave blank)	2. REPORT DATE August 2004	3. REPORT TYPE AND DATES COVERED Annual (15 Jul 2003 – 14 Jul 2004)	

4. TITLE AND SUBTITLE
Automated Area Beam Equalization Mammography for Improved Imaging of Dense Breast

5. FUNDING NUMBERS
DAMD17-03-1-0541

6. AUTHOR(S)
Sabee Molloi, Ph.D.

7. PERFORMING ORGANIZATION NAME(S) AND ADDRESS(ES)
The University of California
Irvine, California 92697-7600

E-Mail: symolloi@uci.edu

8. PERFORMING ORGANIZATION REPORT NUMBER

9. SPONSORING / MONITORING AGENCY NAME(S) AND ADDRESS(ES)
U.S. Army Medical Research and Materiel Command
Fort Detrick, Maryland 21702-5012

10. SPONSORING / MONITORING AGENCY REPORT NUMBER

11. SUPPLEMENTARY NOTES

12a. DISTRIBUTION / AVAILABILITY STATEMENT
Approved for Public Release; Distribution Unlimited

12b. DISTRIBUTION CODE

13. ABSTRACT (Maximum 200 Words)

In mammography, dense breast regions persistently suffer from reduced contrast-to-noise ratio (CNR) because of degraded contrast from large scatter intensities and relatively high noise. Area x-ray beam equalization can improve image quality by increasing the x-ray exposure to under-penetrated regions without increasing the exposure to other breast regions. Optimal equalization parameters with respect to image quality and patient dose were determined through computer simulations and validated with experimental observations on a step phantom and an anthropomorphic breast phantom. Three parameters important in equalization digital mammography were considered: attenuator material (Z=13 to 92), beam energy (22 to 34 kVp), and equalization level. A Mo/Mo digital mammography system was used for image acquisition. A prototype 16x16 piston driven equalization system was used for preparing patient-specific equalization masks. Simulation studies showed that a molybdenum attenuator, a tube voltage of approximately 26-28 kVp, and an equalization level of 20 were optimal for improving contrast, CNR, and figure of merit (FOM=CNR^2/exposure). Experimental measurements using these parameters showed significant improvements in contrast, CNR, and FOM. Moreover, equalized images of a breast phantom showed improved image quality. These results indicate that area beam equalization can improve image quality in digital mammography.

14. SUBJECT TERMS
x-ray imaging, mammography

15. NUMBER OF PAGES
24

16. PRICE CODE

17. SECURITY CLASSIFICATION OF REPORT	18. SECURITY CLASSIFICATION OF THIS PAGE	19. SECURITY CLASSIFICATION OF ABSTRACT	20. LIMITATION OF ABSTRACT
Unclassified	Unclassified	Unclassified	Unlimited

Table of Contents

INTRODUCTION: Mammograms, especially those of dense breasts, incorporate both overexposure in the periphery and underexposure in the dense glandular tissues. Over- and underexposure in these regions degrade their contrast in a film/screen system because these exposures fall in the nonlinear shoulder and heel portions of the film characteristic curve. Moreover, scatter from both the peripheral breast and air gap between the compression paddles significantly reduces the contrast to noise ratio (CNR) and general image quality of mammograms. The overall objective of the proposal is to develop an x-ray beam equalization technique for mammographic applications. Methods under investigation include the design and construction of an x-ray equalization system that reliably generates patient specific templates within a short time interval. The improvement of the overall image contrast-to-noise (CNR) and microcalcification detection, using automated x-ray beam equalization, is evaluated.

BODY: We have done extensive spectral simulation of x-ray beam equalization for mammography. Our beam equalization device was modified for mammography applications. The results of spectral simulations were tested using physical phantoms. This included CNR, FOM and microcalcification detectability. The results have been reported and a reprint is included in the Appendix[1].

KEY RESEARCH ACCOMPLISHMENTS:

- Modification of x-ray beam equalization system for mammography
- CNR measurements using physical phantoms
- Evaluation of microcalcification detectability using physical phantoms

REPORTABLE OUTCOMES:

1. Wong J, Xu T, Husain A, Le H, Molloi S, "Effect of area x-ray beam equalization on image quality and dose in digital mammography" Physics in Medicine and Biology, 49:3539-3557, 2004.
2. Wong J, Xu T, Husain A, Le H, Molloi S: "Effect of area beam equalization on image quality and dose in digital mammography". Medical Physics 31(6):1712, 2004.

CONCLUSIONS: The results of x-ray beam equalization studies showed that the ideal material to use for an attenuator in a Mo/Mo mammography system is molybdenum ($Z = 42$). The use of a molybdenum-based mask material in this study was shown to maintain image contrast with increasing mask thickness. An equalization level of 20 was chosen based on contrast, average glandular dose and tube loading considerations. This study shows that area beam equalization can improve FOM in all regions of the breast. Area beam equalization in digital mammography can reduce patient dose while maintaining adequate CNR throughout the entire breast for lesion detection. It is expected that area beam equalization will improve the detection of nodules and micro-calcifications. A careful receiver operating characteristic (ROC) study needs to be conducted to quantify the improvement in micro-calcification and nodule detection with area beam equalization for thick and dense breasts. Moreover, similar equalization optimization studies for rhodium and tungsten anode systems and different breast thicknesses need to be performed.

REFERENCES:

1. Wong J, Xu T, Husain A, Le H, Molloi S, "Effect of area x-ray beam equalization on image quality and dose in digital mammography" Physics in Medicine and Biology, 49:3539-3557, 2004.

APPENDICES: A reprint of the paper in Physics in Medicine and Biology is included in the Appendix.

PERSONNEL:

Sabee Molloi, Ph.D.
Tong Xu, Ph.D.

Students involved in the project:

Jerry Wong, M.S.
Huy Le
Adeel Husain

Effect of area x-ray beam equalization on image quality and dose in digital mammography

Jerry Wong, Tong Xu, Adeel Husain, Huy Le and Sabee Molloi

Department of Radiological Sciences, University of California, Irvine, CA 92697, USA

E-mail: SYMOLLOI@UCI.EDU

Abstract

In mammography, thick or dense breast regions persistently suffer from reduced contrast-to-noise ratio (CNR) because of degraded contrast from large scatter intensities and relatively high noise. Area x-ray beam equalization can improve image quality by increasing the x-ray exposure to under-penetrated regions without increasing the exposure to other breast regions. Optimal equalization parameters with respect to image quality and patient dose were determined through computer simulations and validated with experimental observations on a step phantom and an anthropomorphic breast phantom. Three parameters important in equalization digital mammography were considered: attenuator material ($Z = 13$–92), beam energy (22–34 kVp) and equalization level. A Mo/Mo digital mammography system was used for image acquisition. A prototype 16×16 piston driven equalization system was used for preparing patient-specific equalization masks. Simulation studies showed that a molybdenum attenuator and an equalization level of 20 were optimal for improving contrast, CNR and figure of merit (FOM = CNR^2/dose). Experimental measurements using these parameters showed significant improvements in contrast, CNR and FOM. Moreover, equalized images of a breast phantom showed improved image quality. These results indicate that area beam equalization can improve image quality in digital mammography.

1. Introduction

In mammography, low-contrast signals from either breast tumours or micro-calcifications have to be visualized. Digital detectors with improved dynamic range and contrast as compared to screen-film have been developed. However, digital detectors can still be overwhelmed by the large variations in transmitted x-ray intensity through thick or dense breasts. A previous study has shown that a dynamic range of 3100 is required to image a 5 cm breast using a tungsten

target x-ray tube (Maidment *et al* 1993). This requirement can increase many times and exceed the dynamic range of current clinically implemented digital mammography detectors, which ranges from 4000 (Tesic *et al* 1997) to 8000 (Muller 1999), when imaging thicker or denser breasts, especially if a Mo or Rh x-ray tube is used. In addition, thicker or denser breast regions persistently suffer from reduced contrast-to-noise ratio (CNR) because of degraded contrast from large scatter intensities and relatively high noise. Such low CNR makes low contrast tumours and micro-calcifications extremely difficult to detect and usually results in additional imaging and dose risk.

X-ray beam equalization can potentially improve CNR in digital mammography by reducing the dynamic range of the detected x-ray intensity. A clinically practical method must be inexpensive, require nominal tube loading, allow for fast image acquisition (<5 s) and not increase average glandular dose significantly above the dose required for conventional mammograms (~1.5 mGy) (LaVoy *et al* 2002). Various approaches for mammographic x-ray beam equalization have been previously reported (Sabol *et al* 1993a, 1993b, Sabol and Plewes 1996, Sabol *et al* 1996, Kwok Leung and Heang-Ping 1990, Goodsitt *et al* 1998, Keshavmurthy *et al* 1999, Panayiotakis *et al* 1998). Previously reported x-ray beam equalization techniques can be divided into scanning equalization and area beam equalization techniques. Scanning equalization systems improve image quality and dose efficiency, but suffer from long scan times and substantial tube loading (Sabol *et al* 1993a, 1993b, Sabol and Plewes 1996, Sabol *et al* 1996). Area beam equalization provides the benefits of short x-ray imaging time and reduced tube loading. However, previous area beam equalization mammography techniques have been limited by non-ideal filter materials (Kwok Leung and Heang-Ping 1990, Keshavmurthy *et al* 1999) as well as filter-breast misalignment and long filter positioning time (Goodsitt *et al* 1998, Keshavmurthy *et al* 1999). These studies have reported comparable, but more uniform, dose to the breast after beam equalization as compared to conventional mammography.

Multi-parameter optimization techniques for image quality and dose in mammography have been studied in depth (Motz and Danos 1978, Jennings *et al* 1981, Beaman and Lillicrap 1982, Muntz *et al* 1985, Fahrig and Yaffe 1994a, 1994b, Court and Speller 1995, Huda *et al* 2003, Ogden *et al* 2003, Berns *et al* 2003). However, previous studies on image quality improvements from mammographic area beam equalization have been presented only qualitatively. There have been no previous reports on the optimization of attenuator material, tube voltage and equalization level for area beam equalization in digital mammography. Furthermore, the effect of equalization on average glandular dose has not been studied.

Previously, an area beam equalization technique was applied to coronary angiography and chest radiography to improve CNR and reduce scatter fraction in the under-penetrated regions of the image (Molloi *et al* 1999, 2001, Xu *et al* 2004). In this study, the optimal equalization parameters for digital mammography were determined using computer spectra simulation. The optimized equalization parameters were then implemented in the prototype equalization system to test the improvement in contrast and CNR for a given dose risk. Furthermore, an estimated average glandular dose after equalization was calculated from the initial unequalized image of the breast and thickness profile of the corresponding equalization mask.

2. Materials and methods

2.1. Image acquisition

All images were acquired using a Profile-2000 mammography system (Trex Medical Corporation, Bennett Division, Copiague, NY) and a focused Bucky grid (5:1 ratio,

31 lines cm^{-1}). The Profile-2000 mammography system consists of a M-2000G single-phase input high-frequency (100 kHz resonant) x-ray generator, molybdenum target and 21.5 μm inherent molybdenum filter (Mo/Mo). The x-ray generator has a 22–35 kVp range with nominal focal spot sizes of 0.1 mm and 0.3 mm depending on kVp and mA. The Profile-2000 mammography system has a linear x-ray output in the experimental range of 8–280 mAs with an entrance exposure of 9.29 mR mAs^{-1} measured 75 cm from the focal spot. As part of this study, the original film screen of the Profile-2000 system was replaced with a PaxScan 4030A amorphous silicon digital x-ray detector (Varian Medical Systems, North Charleston, SC). The PaxScan 4030A digital detector uses columnar CsI:Tl conversion screen technology. It has a 40 × 30 cm^2 effective detection window with a 194 μm pixel pitch, corresponding to a limiting resolution of 2.58 lp mm^{-1}. The PaxScan 4030A has a linear response for detected intensities up to a pixel value of 8500 at a detector gain of 1, which corresponds to a detector entrance exposure of 91 mR (28 kVp, 10.4 mAs). The source to image receptor distance (SID) was set at 75 cm.

2.2. Prototype area beam equalization system

The prototype equalization system uses a patient-specific attenuation mask to modulate the x-ray beam intensity spatially before it reaches the breast so that x-ray flux after the breast is approximately equalized. The equalization mask is made from a mixture of a deformable attenuation material comprising a poly-dimethylsiloxane binder (Depco Inc., Hauppauge, NY) and molybdenum powder (Atlantic Equipment Engineers, Bergenfield, NJ) in an 8.6:1 binder to molybdenum powder weight/weight ratio. Areas corresponding to the low attenuating regions in the open field and around the nipple have thicker filters than areas corresponding to high attenuating regions near the chest wall. The equalization device provides a maximum mask thickness of 8.4 mm, which reduces the incident 28 kVp x-ray intensity by a factor of 55.

A flow chart and diagrams of the equalization device and area beam equalization mammography system are shown in figures 1 and 2. An initial low dose (pre-exposure) image of the breast is acquired with the digital detector and converted to an 8 bit (255 grey level), 2 × 2 binned image. The resulting digital image is then segmented into a matrix of 16 × 16 square regions where the grey levels are transformed to derive a two-dimensional thickness profile of the equalization mask. The mask thickness in cm (τ_A) for each matrix square is calculated from each region's average primary x-ray intensity (I_{region}), maximum average primary intensity in the image (I_{max}) and reduction magnitude of the primary intensity, henceforth known as equalization level (EQ):

$$I_{\mathrm{target}} = \frac{I_{\mathrm{max}}}{\mathrm{EQ}} \tag{1}$$

$$Ratio = \frac{I_{\mathrm{region}}}{I_{\mathrm{target}}} \tag{2}$$

$$\tau_A = 0 \qquad \text{if} \quad Ratio \leqslant 1 \tag{3}$$

$$\tau_A = \frac{1}{\mu_0} \ln(Ratio) + \alpha[\ln(Ratio)]^2 \qquad \text{if} \quad Ratio > 1. \tag{4}$$

Equation (4) is used to calculate the mask thickness, where μ_0 is the linear attenuation coefficient of the material. Due to the beam hardening effect, the mask thicknesses and the natural logarithm of the attenuation ratio ($Ratio$) show a nonlinear relationship. A nonlinear term $\alpha[\ln(Ratio)]^2$ was added to account for this effect. Attenuation ratios for different
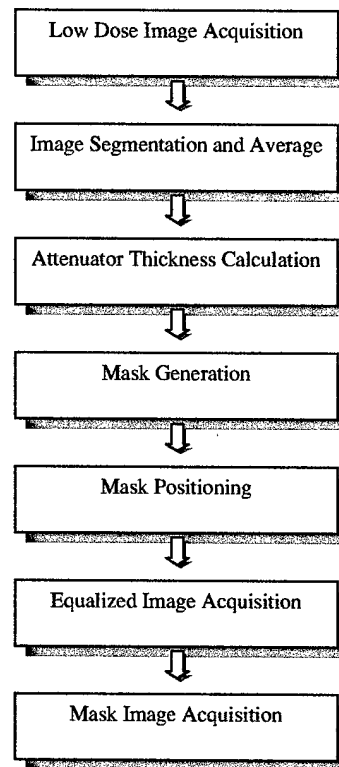
Figure 1. Flow chart for an area x-ray beam equalization system for digital mammography.

mask thicknesses were known from spectra modelling and were shown to agree well with experimentally determined attenuation ratios at 0.2, 0.4, 0.6 and 0.8 cm of mask thickness. The coefficients for equation (4) are derived by a regression between the mask thicknesses and the natural logarithm of *Ratio*. For this mixture of attenuating material, the coefficients μ_0 and α for calculating the mask thicknesses are 6.06 cm^{-1} and 0.0105 cm, respectively.

An array of 16 × 16 square pistons, with dimensions of 0.159 × 0.159 cm^2, is used to shape the mask material. The pistons are pushed into the material row by row using 16 stepper motors. An equalization mask with the desired two-dimensional thickness profile is generated by controllably pushing down on the mask to a target depth with the 256 pistons. After the mask is generated, it is separated from the pistons and manually positioned immediately below the collimator of the mammography system on a fixed mask holder mount to achieve the largest breast coverage on the flat panel detector. The distance between the mask holder and the focal spot is 12.5 cm. The actual position calibration of the mask is described in detail elsewhere (Molloi *et al* 2001).

With the mask in place, the equalized image is acquired. However, this image will contain artefacts from the mask because of the limited spatial resolution of the pistons. In order to minimize mask artefacts, an image of the mask without the breast is acquired and subtracted from the equalized image. To minimize noise contribution from the subtraction, this mask
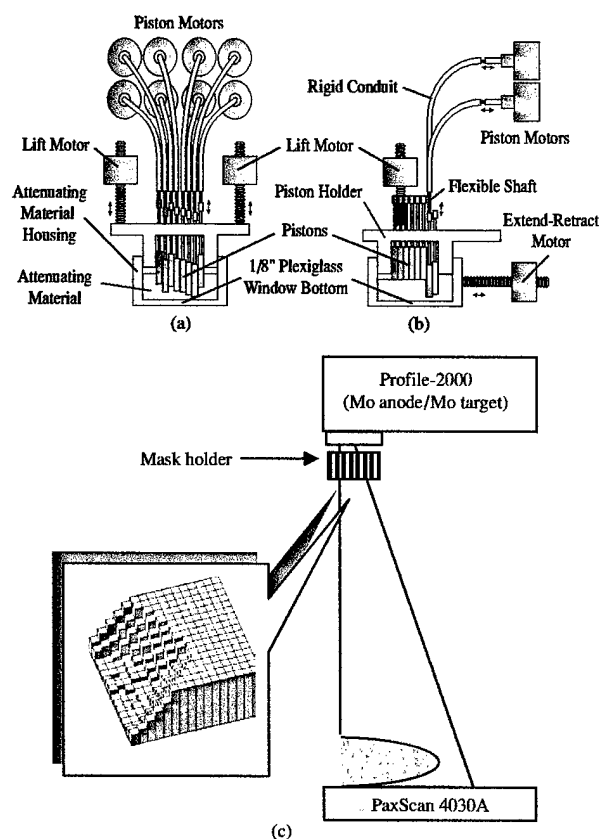
Figure 2. (a) Front view and (b) side view of the prototype device used to generate attenuation masks. (c) A diagram of area x-ray beam equalization applied to mammography. The equalization filter was fabricated by the equalization device and manually positioned in the x-ray beam at 12 cm from the focal spot. A magnified view of the 16×16 equalization mask is shown. The cross-sectional area of the filter is 2.54 × 2.54 cm^2 and SID is 75 cm.

image is smoothed by a 3 × 3 pixel (0.6 mm) running average kernel (Dobbins and Powell 1989). The blurred mask image is not expected to introduce any visible artefact because of the 2 mm focal spot blurring of the mask image. A detailed description of the prototype area beam equalization system has been reported elsewhere (Molloi *et al* 2001, Xu *et al* 2004).

2.3. Simulation studies

A computer simulation program was written based on a previously reported technique to generate a molybdenum anode mammography spectrum with 0.5 keV bins (Boone *et al* 1997). A library of energy-dependent mass attenuation coefficients based on published data was used to calculate the resultant transmission through various materials. Simulation studies were designed to mimic experimental conditions (elemental compositions and thicknesses of the inherent filter, equalization mask, phantoms and detector components) closely (table 1). X-ray

Table 1. Simulation and experimental parameters.

X-ray source	Mo anode, 21.5 μm Mo, 1 mm Be
Source to detector distance	75 cm
Detectors	PaxScan 4030A
	Scintillator: 0.6 mm CsI
	Pixel size: 194 × 194 μm^2
	Protection layer: 2.5 mm carbon fibre, 0.25 mm Al
	Digital mammography detector (simulation only)
	Scintillator: 0.2 mm CsI
	Pixel size: 100 × 100 μm^2
	Protection layer: 2.5 mm carbon fibre, 0.25 mm Be
Step phantom	Material: BR12
	Steps: 50 mm, 30 mm and 15 mm
Contrast object	4.8 × 10 × 10 mm^3 Lucite

scatter was not included in the simulation. Relative noise (RN) was assumed to depend only on quantum noise and all other sources of noise were assumed to be negligible. The initial simulated x-ray intensity is also normalized to the experimental entrance exposure.

Simulation studies were conducted to quantify scatter-free contrast, relative CNR, average glandular dose (AGD) and figure of merit (FOM = CNR^2/AGD) with and without area beam equalization in digital mammography. Contrast and CNR measure image quality, whereas FOM quantifies improvements in image quality per dose risk to the patient (Ogden *et al* 2003, Zamenhof 1982, Boone 1992, Huda *et al* 1998, Dobbins *et al* 2003). By defining FOM as CNR^2/AGD, FOM becomes independent of patient dose and the optimization process is simplified because mAs, entrance exposure or dose do not need to be considered. To validate that the simulation data will reflect experimental results within an acceptable error, numerous simulation values such as half value layer of aluminium (HVL), contrast and CNR were compared to their corresponding experimental values and the error was evaluated. Since experimental noise is difficult to simulate accurately, changes in CNR and FOM due to breast thickness, kVp and equalization were calculated relative to a reference CNR$_0$ and FOM$_0$ obtained under the following conditions: the Lucite contrast object (4.8 mm) was placed on 50 mm BR12 and imaged at 28 kVp and 9.6 milliampere seconds (mAs) with no grid and no equalization. The calculation of AGD is explained in section 2.5.

2.3.1. Optimization of equalization parameters. Computer simulations were initially conducted to determine optimal parameters such as material, kVp and equalization level for area beam equalization using two different detectors as listed in table 1. First, contrast and relative CNR after equalization with different mask materials composed of a poly-dimethylsiloxane binder and different elements ranging from atomic numbers $Z = 13$ (aluminium) to $Z = 92$ (uranium) were calculated to select an attenuator that would give the best contrast with equalization. For each Z, an appropriate mask thickness satisfying equations (1)–(4) for a given equalization level was calculated with an iterative root-finding algorithm called the bisection method. Second, the dependence of contrast, relative CNR and relative FOM on kVp was investigated. Third, contrast, relative CNR and relative FOM for different equalization levels were calculated to determine an optimal equalization level based on image quality improvements versus increased exposure and tube loading considerations. In simulating a clinical digital mammography detector, the thin protective layer of aluminium found in the PaxScan 4030A detector was substituted with beryllium ($Z = 4$) so that the

attenuation of low energy photons is reduced and higher contrast and CNR as required in mammography are provided.

2.4. Experimental studies

Analysis of simulation results revealed the optimal attenuation material, kVp and equalization level for experimental studies on contrast, CNR and FOM in equalization digital mammography. A tube voltage of 28 kVp and an equalization level of 20 were chosen. Unless stated otherwise, images were acquired at 28 kVp and an equalization level of 20 was used for equalized images. Tube loading (mAs) for unequalized images was chosen to give maximal detector signal (7000–8000) without saturation in the open field. With equalization, the mAs was increased to compensate for the mask attenuation. The tube loading for unequalized and equalized images was chosen to be 9.6 mAs and 128 mAs, respectively. Such a large increase in mAs with equalization was used to explore the maximum image quality improvement without dose considerations because CNR can be estimated for any dose level when operating within the quantum limited region. A step phantom made of breast tissue equivalent material (BR12, GAMMEX RMI, Middleton, MI) was used for image quality evaluation. BR12 is a homogenous material that mimics the attenuation properties of average density breast with 50% glandular/50% adipose breast tissue over the range of energies used in mammography. The step phantom consisted of 15 mm, 30 mm and 50 mm steps with edges 10 mm apart. A compressed anthropomorphic breast phantom (Caldwell and Yaffe 1990) was used to test the equalization system and evaluate dose under clinically relevant conditions.

The equalization process involves acquiring a pre-exposure image and generating a patient-specific mask with the equalization device shown in figure 2. Prior to generating the mask, the pre-exposure image is corrected for scatter (Molloi and Mistretta 1988). The original pre-exposure image is convoluted with a Gaussian-shaped scatter profile corresponding to a full-width at half-maximum (FWHM) of 2 cm (Boone *et al* 2000, Cooper *et al* 2000). Scatter fraction as a function of grey level is determined by measuring the scatter fraction for different thicknesses of BR12 (Molloi and Mistretta 1988). A scatter image is obtained from multiplying the blurred image with the scatter fraction image. The scatter image is subtracted from the original image to obtain a primary only image. The grey levels from this primary only image are used to generate the patient-specific mask. Scatter fraction (SF), contrast, CNR and FOM were determined for a step phantom under four conditions: (1) no grid and no equalization, (2) no grid but with equalization, (3) with grid but no equalization and (4) with grid and with equalization.

2.4.1. Half value layer.
The beam quality in terms of HVLs of aluminium for 26, 28 and 30 kVp incident beams and HVLs for a 28 kVp beam attenuated with 3.4 mm, 5.0 mm and 7.0 mm of the molybdenum-based attenuation material were determined with a 6 cm^3 mammography ion chamber (Model 20X6–6M-3, Radcal Corporation, Monrovia, CA).

2.4.2. Scatter fraction.
Scatter fractions were determined with the conventional beam stop method (Molloi *et al* 1998). Two images with and without lead discs were acquired for each scatter fraction measurement. Using a 10 pixel diameter circular region of interest (ROI), scatter fractions were determined from the ratios of pixel intensities at the centre of a lead disc and at the identical location without the lead disc. Scatter fractions were determined using lead discs with diameters 9.40 mm, 6.56 mm, 4.12 mm and 2.50 mm. The scatter fraction at a zero lead disc diameter was then extrapolated from a linear regression analysis.

2.4.3. Contrast. The image contrast due to a Lucite block ($4.8 \times 10 \times 10$ mm^3) was determined from images with and without the Lucite block. Average detected intensities within a defined 10×10 pixel square ROI covering a 100 pixel area at the centre of the Lucite block (I_{Lucite}) and at the same location without the Lucite block ($I_{background}$) were determined. Contrast for the Lucite block was then calculated according to equation 5(a). Contrasts for the Lucite block placed along the step edges at 15, 30 and 50 mm of BR12 were calculated. In order to compare to simulation results, experimental contrast was corrected for scatter according to equation 5(b):

$$\text{Contrast}_{exp} = \frac{I_{background} - I_{Lucite}}{I_{background}} \tag{5a}$$

$$\text{Contrast} = \frac{\text{Contrast}_{exp}}{(1 - SF)}. \tag{5b}$$

2.4.4. Contrast-to-noise ratio. In calculating CNR for the Lucite block on the step phantom, relative noise was first determined. Two images of the step phantom were acquired under identical conditions. The images were then linearly subtracted to remove position-dependent non-uniformities that can affect the relative noise values. The standard deviation (σ) within a 10×10 square ROI of the subtracted image was determined and adjusted by $1/\sqrt{2}$ to account for the additive quantum noise from image subtraction. The experimental CNR and the scatter corrected CNR are computed from the following equations:

$$\text{CNR}_{exp} = \frac{I_{background} - I_{Lucite}}{\sigma} \tag{6a}$$

$$\text{CNR} = \frac{\text{CNR}_{exp}}{\sqrt{1 - SF}}. \tag{6b}$$

In the quantum limited region, CNR is proportional to $\sqrt{mAs}$, so CNR can also be adjusted for different tube loading.

2.4.5. Figure of merit. FOM was calculated from the square of CNR divided by the average glandular dose. Average glandular dose is calculated from the normalized average glandular dose ($\bar{D}_{gN}$) and entrance exposure (X_{ESE}). The approximation of average glandular dose is discussed in detail in the next section. Entrance exposures without equalization were measured with a mammography ion chamber. These entrance exposure values were then used to predict entrance exposures after different thicknesses of mask material using the simulation program.

2.5. Average glandular dose approximation

Average glandular dose ($\bar{D}_g$) with and without equalization was computed from the product of the normalized average glandular dose ($\bar{D}_{gN}$) and entrance skin exposure (X_{ESE}):

$$\bar{D}_g = \bar{D}_{gN} \cdot X_{ESE} \tag{7}$$

$\bar{D}_{gN}$ is a function of kVp, HVL, breast thickness and breast composition. It was determined semi-empirically following a previously reported method (Sobol and Wu 1997). $\bar{D}_g$ is usually calculated for a uniform thickness of compressed breast with the periphery ignored. However, equalization reduces the dose to the periphery and this effect has to be evaluated. This requires

the knowledge of the distribution of breast thickness and entrance exposure. Thus, the average glandular dose of the entire breast can be calculated from the sum of all pixilated $\bar{D}_{g,i}$ within an ROI in the mammogram weighted by the fraction of the breast mass in each pixel (w_i) to the total breast mass (w_{total}):

$$\bar{D}_g = \sum_i \bar{D}_{g,i} \cdot \left(\frac{w_i}{w_{\text{total}}}\right) = \sum_i \bar{D}_{\text{gN},i} \cdot X_{\text{ESE},i} \cdot \left(\frac{w_i}{w_{\text{total}}}\right). \tag{8}$$

The breast thickness for each pixel (d_i) is derived from the mammogram. Assuming the effective linear attenuation coefficient of the breast phantom is not significantly affected by beam hardening, a breast thickness image can be derived from the unequalized mammogram. The HVL_i for the unequalized beam is constant at 0.28 mm aluminium. In the case of equalization, HVL_i increases as a function of mask thickness in cm (τ_A) according to the following best-fit polynomial to simulation data:

$$\text{HVL}_i = -2.0105\tau_A^4 + 4.3363\tau_A^3 - 3.4941\tau_A^2 + 1.3847\tau_A + 0.2807 \tag{9}$$

X_{ESE} is calculated from the initial exposure $\left(X_{\text{ESE}}^o\right)$ and its attenuation due to a mask of thickness τ_A with an effective linear attenuation coefficient $\mu_{\text{Mask}}^{\text{eff}}$:

$$X_{\text{ESE}} = X_{\text{ESE}}^o \exp\left(-\mu_{\text{Mask}}^{\text{eff}} \cdot \tau_A\right) \tag{10}$$

$\mu_{\text{Mask}}^{\text{eff}}$ was determined to be 6.044 cm^{-1}. A program was written that uses input images of the breast and mask and creates a weighted average glandular dose image. An ROI around the breast region can be drawn manually. The total sum within this ROI gives the average glandular dose $\bar{D}_g$ of the breast.

The above parametrization method assumes a uniform compressed breast for a limited range of breast thicknesses (3–8 cm) and HVLs (0.24–0.43). In an effort to calculate the average glandular dose, it was assumed that the $\bar{D}_{\text{gN}}$ values near the nipple area are reasonably close to values of uniform breasts of the same thickness. In addition, $\bar{D}_{\text{gN}}$ was extrapolated for breast thicknesses and HVLs outside the original tabulated ranges (Wu et al 1991). This extrapolation introduces acceptable errors because $\bar{D}_{\text{gN}}$ depends linearly on HVL and bi-exponentially on breast thickness. A previous report has indicated that the errors associated with extrapolated $\bar{D}_{\text{gN}}$ for breast thicknesses down to zero could be up to 15% (Sobol and Wu 1997).

3. Results

3.1. Simulation studies

Simulated and experimental contrast and relative CNR behaved similarly. Figure 3 shows that experimental and simulated PaxScan 4030A and clinical digital mammography detector contrast decreased linearly per unit increase in kVp by approximately 0.92%, 0.98% and 0.85%, respectively. Moreover, figure 4 shows that experimental and simulated contrast and relative CNR for different thickness of BR12 are in good agreement.

3.1.1. Optimization of equalization parameters.
Simulated contrasts for a level 20 equalization of 15 mm of BR12 as a function of mask material $(Z = 13$ to $Z = 92)$ for 24, 26, 28 and 30 kVps are shown in figure 5(a). Contrast generally decreases with kVp for all the materials. However, an increase in contrast was observed at around $Z = 42$ (Mo) for all kVps. Figure 5(b) shows simulated contrasts for an equalized 15 mm BR12 using 28 kVp as a function of different mask materials for equalization levels 5–40. Contrast remained fairly
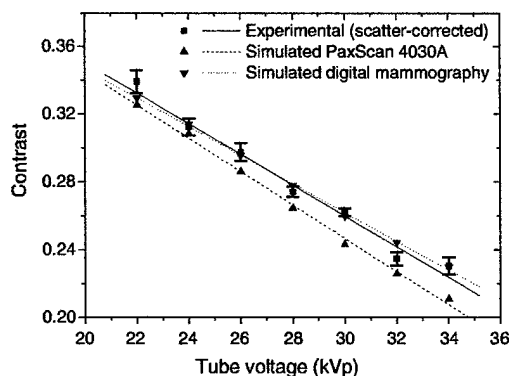
Figure 3. Experimental and simulated contrast as a function tube voltage for a 4.8 mm thick Lucite contrast object on 50 mm BR12. Experimental and simulated PaxScan 4030A and clinical digital mammography detector contrasts decrease linearly with kVp by approximately 0.92%, 0.98% and 0.85%, respectively, per unit increase in kVp. The error bars represent a 95% confidence interval determined from error analysis of five repeated measurements.
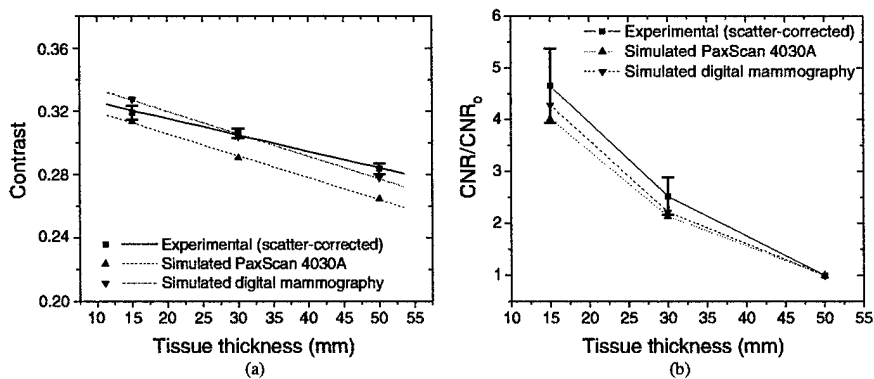

Figure 4. A comparison between experimental and simulated (a) contrast and (b) relative CNR. Measurements were performed using 14 × 14 cm BR12 slabs and a 4.8 mm thick Lucite contrast object. The images were acquired using 28 kVp, 9.6 mAs, 75 cm SID and no equalization. The error bars represent a 95% confidence interval determined from error analysis of five repeated measurements.

constant and even increased with increasing levels of equalization near $Z = 42$. However, contrast can decrease up to 17% for $Z < 35$ and $Z > 48$ (e.g. from 0.306 to 0.254 for $Z = 13$). Further simulations for an actual mask made from 8.6:1 wt/wt ratio of the binder material and molybdenum showed that contrast remained relatively constant up to an equalization level of 48 (figure 6). Figure 7 shows the results for the optimization of relative FOM with kVp and equalization level for 15 mm and 30 mm of BR12. Relative FOM shows a maximum for equalized 15 mm BR12 at 26 kVp for equalization levels 10 and higher. For equalized 30 mm BR12, relative FOM shows a maximum at 26, 28 and 30 kVp for equalization levels 40, 20 and 10, respectively. There was no observed local maximum in relative FOM within the 22–34 kVp range for 50 mm BR12 because of the thick (600 μm) CsI scintillator.
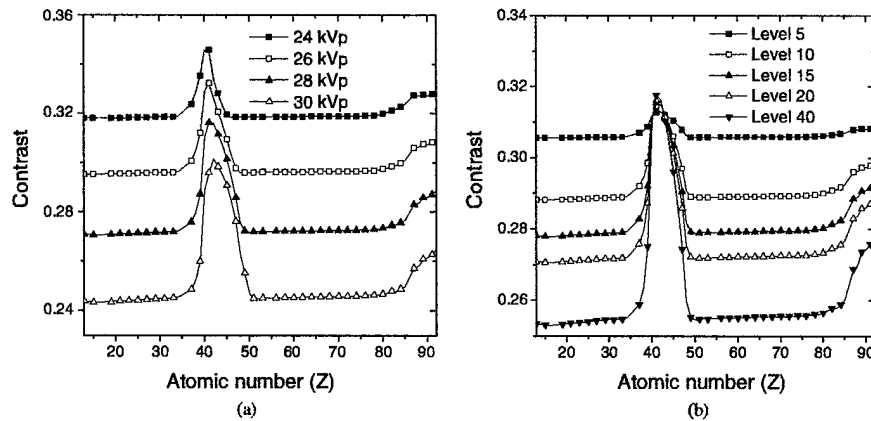
Figure 5. Simulated contrast versus attenuators made from different Z materials for the Lucite contrast object on 15 mm BR12 for (a) different kVps (level = 20) and (b) different equalization levels (kVp = 28). Entrance exposure to the 50 mm region of the step phantom was kept constant at 100 mR.
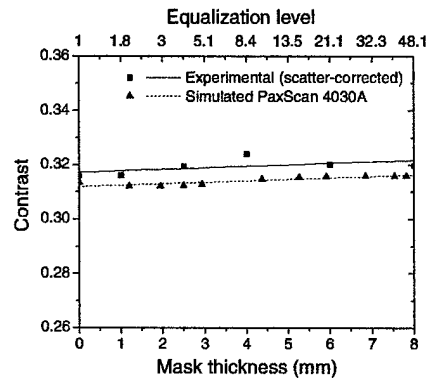

Figure 6. Scatter-corrected experimental and simulated contrast versus mask thickness for the Lucite contrast object imaged on the 15 mm region of the step phantom. Images were acquired at 28 kVp. Slopes of the scatter-corrected experimental and simulated fit lines are 0.00045 and 0.00053, respectively. Scatter-corrected experimental contrast was calculated using a measured scatter fraction of 0.1954 (±0.0009).

Figure 8 shows the improvement in relative FOM with equalization level for 15 mm BR12 imaged at 28 kVp.

3.2. Experimental studies

The equalization system successfully provided beam equalization for both the step and the anthropomorphic breast phantoms. A quantitative evaluation of image quality and dose parameters (such as SF, contrast, CNR, AGD and FOM) on the step phantom are tabulated
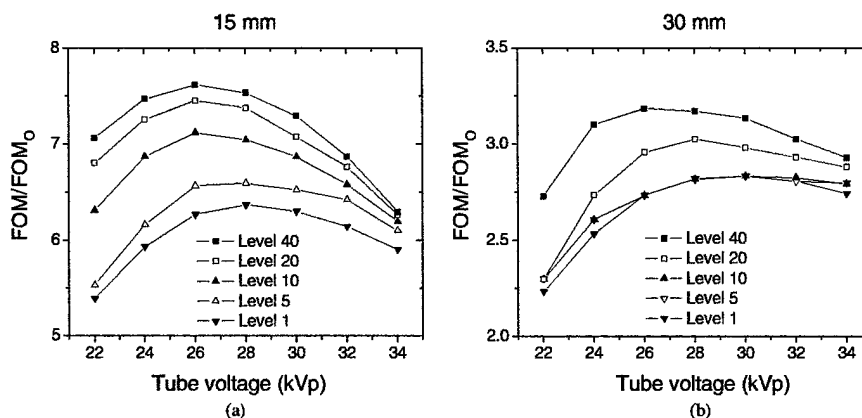
15 mm

30 mm

Figure 7. Simulated relative FOM as a function of tube voltage for the Lucite contrast object on (a) 15 mm BR12 and (b) 30 mm BR12 at various equalization levels. Entrance exposure to the 50 mm region of the step phantom was kept constant at 100 mR.
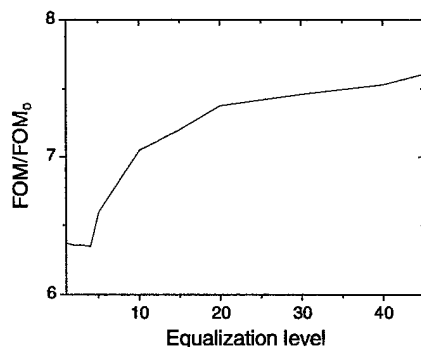

Figure 8. Simulated relative FOM versus equalization level for the Lucite contrast object on the 15 mm region of the step phantom using a tube voltage of 28 kVp. Entrance exposure to the 50 mm region of the step phantom was kept constant at 100 mR.

in tables 3–5. Figures 9(a) and (b) show breast phantom images with simulated micro-calcifications before and after equalization.

3.2.1. Half value layer. Table 2 shows the experimental and simulation HVLs for different kVps and mask thicknesses. The HVLs at 26, 28 and 30 kVp with no mask were determined to be 0.26, 0.28 and 0.29 mm of aluminium and 0.26, 0.28 and 0.30 mm of aluminium for experimental and simulation measurements, respectively. The HVLs at 28 kVp with mask thicknesses of 3.4, 5.0 and 7.0 mm were determined to be 0.48, 0.51 and 0.55 mm of aluminium and 0.49, 0.52 and 0.54 mm of aluminium for experimental and simulation measurements, respectively.
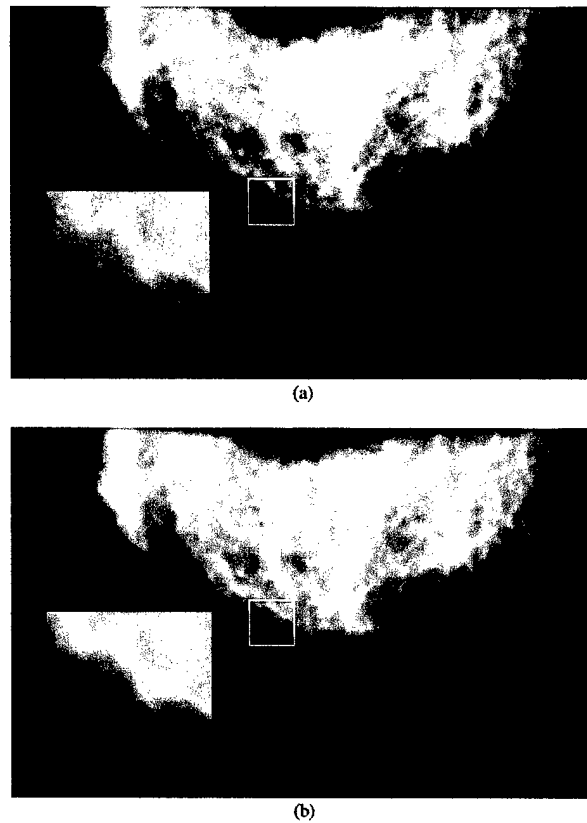
(a)

(b)

Figure 9. (a) An unequalized image taken with 28 kVp and 9.6 mAs. (b) A digital mammographic image of an equalized breast phantom with the mask subtracted. Image was taken with 28 kVp and 72 mAs. The white square encompasses the 3 × 3 array of 180–230 μm micro-calcifications.

Table 2. Experimental and simulated HVLs for different kVps and mask thicknesses.

Energy (kVp)	Mask thickness (mm)	$HVL_{exp.}$ (mm Al)	$HVL_{sim.}$ (mm Al)
26	0.0	0.26	0.26
28	0.0	0.28	0.28
30	0.0	0.29	0.30
28	3.4	0.48	0.49
28	5.0	0.51	0.52
28	7.0	0.55	0.54

3.2.2. Scatter fraction, contrast, CNR and FOM. Tables 3 and 4 show measured scatter fraction, contrast and CNR for different thicknesses of the step phantom without (table 3) and with a grid (table 4). SF generally increased with increasing BR12 thickness. SF on the 15 mm region increased slightly when equalization was applied without grid. SF on

Table 3. Experimental scatter fraction, contrast and CNR for the step phantom imaged without a grid. Unequalized and equalized images were acquired at 9.6 mAs and 128 mAs, respectively. A 95% confidence interval is shown ($n = 5$).

BR12	Unequalized			Equalized		
(mm)	SF	Contrast	CNR	SF	Contrast	CNR
15	0.174 ± 0.004	0.264 ± 0.003	68 ± 6	0.206 ± 0.005	0.252 ± 0.001	109 ± 6
30	0.274 ± 0.004	0.222 ± 0.002	34 ± 2	0.252 ± 0.004	0.230 ± 0.001	100 ± 10
50	0.448 ± 0.005	0.157 ± 0.001	12 ± 1	0.333 ± 0.004	0.184 ± 0.006	58 ± 4

Table 4. Experimental scatter fraction, contrast and CNR for the step phantom imaged with a grid. Unequalized and equalized images were acquired at 20 mAs and 280 mAs, respectively. Error analysis was not performed because subtle grid artefacts were visible at high magnification.

BR12	Unequalized			Equalized		
(mm)	SF	Contrast	CNR	SF	Contrast	CNR
15	0.152	0.261	59	0.146	0.296	127
30	0.205	0.242	35	0.148	0.267	107
50	0.276	0.215	16	0.193	0.217	83

Table 5. CNR, AGD and relative FOM for a step phantom (without grid) adjusted to a same tube loading as that used for the unequalized image (9.6 mAs). Relative FOM is normalized with FOM_0 at 50 mm BR12, 28 kVp, 9.6 mAs, no grid and no equalization.

BR12	Unequalized			Equalized		
(mm)	CNR	mGy	Relative FOM	CNR	mGy	Relative FOM
15	68	0.32	13	30	0.059	14
30	34	0.21	5.0	27	0.12	5.5
50	12	0.13	1.0	16	0.13	1.8

the 50 mm region is significantly reduced when equalization was applied either with or without grid. Contrast was improved with equalization. This was particularly apparent in the thickest part of the phantom where contrast increased from 15.7% when no equalization and no grid were used to 21.7% when both equalization and grid were used. CNR increased with equalization for all thicknesses of the step phantom with and without a grid. The largest improvement with equalization was in the 50 mm BR12 region where CNR increased from 12 to 58 and 16 to 83 without and with grid, respectively. Improvements in CNR were due to both increased contrast and reduced quantum noise after beam equalization. An analysis of the effect of equalization alone is given in table 5 where CNR, AGD and FOM for the step phantom (without grid) have been adjusted to a same tube loading as that used for the unequalized image (9.6 mAs). Table 5 shows that equalization greatly reduces dose to the periphery. Average glandular dose for the whole breast phantom without and with equalization at the same tube loading was calculated to be 0.16 mGy and 0.12 mGy, respectively. Although CNR in the 15 mm and 30 mm regions decreased, they are still larger than the CNR in the 50 mm region. FOM values for all regions of the step phantom are shown to increase with equalization.
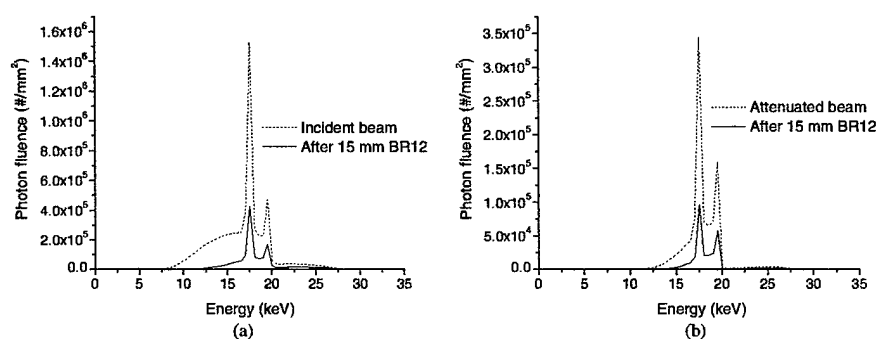
Figure 10. Spectral changes (a) without equalization and (b) with 20 times equalization. The dashed lines (- - -) represent the entrance beam spectra before passing through 15 mm BR12, and the solid lines (—) represent the exiting beam spectra after penetrating through 15 mm BR12.

4. Discussion

4.1. Equalization parameters

4.1.1. Attenuator material.
In area beam equalization, the choice of attenuator material is very important. In addition to modulating the incident x-ray beam, it is also important to simultaneously optimize the x-ray beam spectra. Contrast was used as the primary parameter to optimize attenuation material. This is because both CNR and FOM can be improved with increasing kVp and equalization level. However, contrast would be degraded significantly for all kVp and equalization levels if an inappropriate material, such as aluminium or cerium, were to be used (figures 5(a) and (b)). Most physical attenuators cause beam hardening, which degrades contrast. However, certain k-edge materials are capable of maintaining the same level of contrast or even improve it slightly. Simulation and experimental results show that a molybdenum-based attenuator slightly improved contrast with increasing thickness up to 8 mm of mask material (figure 6), which contains an equivalent of 10.2 μm of pure molybdenum. An inappropriate attenuator material would substantially degrade contrast with increasing mask thickness as demonstrated by figure 5(b).

Our results agree with previous reports on optimal filtration material for mammography (Fahrig and Yaffe 1994b, Calicchia *et al* 1994, 1996). In our study, contrast was observed to remain constant even up to an equalization level of 48, or 8 mm of mask material. The total filtration including the inherent filter (21.5 μm molybdenum) and 8 mm of mask material (10.2 μm molybdenum) was 31.7 μm of molybdenum. Similarly, Calicchia *et al* concluded that image contrast improved slightly with increasing molybdenum filtration up to 45–60 μm (Calicchia *et al* 1994). They also found that for a Mo/Mo system increasing the molybdenum filtration up to 75 μm significantly reduced entrance exposure and dose without loss of image quality for a film-screen system. Fahrig and Yaffe reported that a maximum signal-to-noise ratio (SNR) for a 200 μm calcification was achieved with a filter made from molybdenum for a Mo/Mo system and a Gd$_2$O$_2$S scintillating screen (Fahrig and Yaffe 1994b). Our results show that using molybdenum in the mask material allows area beam equalization to increase the fraction of photons in the 17–20 keV range by preferentially attenuating the lower and higher energy photons (figure 10). Combined contrast enhancement with exposure reduction results from molybdenum filtration, which removes high energy (>20 keV) photons that degrade

contrast and low energy (<17 keV) photons that primarily contribute to radiation risk without significant contribution to image formation.

Molybdenum filter thickness in a Mo/Mo system is chosen in order to reduce patient dose and improve image quality with a tolerable tube loading. Although previous studies on the optimization of inherent filter thickness versus image quality and patient dose have suggested the use of thicker filters, they have not been implemented into clinical systems due to the fact that imaging thick breasts would result in an excessive tube loading. In area beam equalization, however, the benefits of patient dose reduction and image quality enhancement from more optimal filters can be provided within tube loading limitations. This is because area beam equalization provides a spatially variable filter that provides the appropriate filter thickness as a function of breast thickness. In doing so, the aim to narrow the spectrum of incident beam through filtration can be realized in a clinical setting. Image quality can be maximized while minimizing patient dose by utilizing an area beam equalization system that can generate patient-specific masks.

4.1.2. Equalization level. In area beam equalization, no mask material is placed in the region corresponding to the thickest part of the anatomy. By attenuating the regions corresponding to the thinner part of the anatomy, it is possible to increase the incident exposure to the thicker part of the anatomy. Therefore, CNR is increased in the thicker part of the anatomy by the increased incident exposure to this region and reduced cross scatter from the thinner parts of the anatomy (see tables 3 and 4). This will also result in increased tube loading, which might not be practical for thicker breasts. Area beam equalization can then be used to generate an image with more uniform CNR in all regions of the image while maintaining the x-ray tube loading within a practical range.

An important factor in equalization is the changes in incident x-ray exposure after equalization. This can be evaluated using FOM, which normalizes CNR changes with dose changes. It is important to determine the optimal equalization level while minimizing both patient dose and x-ray tube loading. This was done by calculating the FOM for different equalization levels (see figure 8). The results show that FOM increases with increasing equalization level and starts to plateau at an equalization level of 20. This indicates that equalization levels higher than 20 are not justified. The increase in FOM is due to the preferential attenuation of lower energy photons that have very low transmission through the breast, but would have contributed most to breast exposure. Figure 10 shows the change in incident spectrum with and without the equalization mask material. The beam spectrum after the equalization mask more closely resembles the beam exiting the BR12 phantom without equalization. Most of the photons below 10 keV are attenuated, and the photons below 15 keV are greatly reduced. The mask reduces incident patient exposure by preferentially removing photons that do not contribute to image formation and maintains contrast by narrowing the spectrum of the incident beam.

4.2. Image quality and dose

Image contrast is reduced as the detected x-ray scatter is increased. An anti-scatter grid can successfully remove a large component of scatter throughout the image field, but the primary x-ray intensity can also be attenuated by as much as 50%. Equalization can also provide scatter reduction to thick or dense breast regions by equalizing the primary intensity throughout the breast. However, equalization can also slightly increase the scatter fraction to the thinner breast regions because the primary intensities to these regions are reduced by equalization. This effect can be observed from the results for the 15 mm thickness of the step phantom shown

in table 3. The effect of scatter reduction for grid and equalization is cumulative. Equalization produces an image with approximately uniform scatter fraction and the grid reduces scatter in the entire image. Improvements in scatter fraction from using both equalization and grid are shown in table 4. This improvement in scatter fraction and subsequent contrast enhancement is the main reason for the increased FOM in the thickest region.

A pre-exposure image is required for area beam equalization. The pre-exposure image can be acquired with minimal patient dose. For example, the prototype equalization system can acquire a pre-exposure image using 1.3 mAs, which is the lowest possible setting for the mammography system. The image was adequate for calculating the 16×16 array of mask thicknesses. The average glandular dose under these conditions is only 0.02 mGy. It is anticipated that the patient dose can be further reduced by acquiring the initial image at lower mAs than that achievable with the current mammography system. Compared to conventional mammography, area beam equalization has been shown to decrease average glandular dose by 25% for a given incident exposure (from 0.16 mGy to 0.12 mGy). This 25% dose reduction was due to the reduced entrance exposure to the thinner regions, increased beam hardening and selective attenuation of low energy photons that do not contribute to the formation of the image. Thus, it is possible to improve image quality with equalization in mammography without an increase in total breast dose.

4.3. Digital detector

Although the digital detector (PaxScan 4030A) used in this study was not designed for mammography applications, it provided good contrast and CNR for the Lucite contrast object. Simulated results showed that the image contrast and CNR from the PaxScan 4030A digital detector compared reasonably well with the simulated clinical digital mammography detector (figures 3 and 4). Therefore, the observed improvements in contrast and CNR with area beam equalization in this study should apply to studies performed with a clinical digital mammography system.

Another limitation of our digital detector for mammography applications is its spatial resolution of 194 μm as compared with the GE digital detector, which has a pixel size of 100 μm (Muller 1999). This lower spatial resolution was not optimal for detecting <200 μm micro-calcifications. However, the aim of this study was to evaluate the effect of area beam equalization on contrast and CNR. This was successfully accomplished using reasonably large contrast objects. Therefore, it is expected that the visibility of smaller contrast objects such as micro-calcifications and nodules, using a dedicated digital mammography detector, should improve with area beam equalization as demonstrated in this study.

5. Conclusions

The results of x-ray beam equalization studies showed that the ideal material to use for an attenuator in a Mo/Mo mammography system is molybdenum ($Z = 42$). The use of a molybdenum-based mask material in this study was shown to maintain image contrast with increasing mask thickness. An equalization level of 20 was chosen based on contrast, average glandular dose and tube loading considerations. This study shows that area beam equalization can improve FOM in all regions of the breast. Area beam equalization in digital mammography can reduce patient dose while maintaining adequate CNR throughout the entire breast for lesion detection. It is expected that area beam equalization will improve the detection of nodules and micro-calcifications. A careful receiver operating characteristic (ROC) study needs to be conducted to quantify the improvement in micro-calcification and nodule detection with area

beam equalization for thick and dense breasts. Moreover, similar equalization optimization studies for rhodium and tungsten anode systems and different breast thicknesses need to be performed.

Acknowledgment

References

Beaman S A and Lillicrap S C 1982 Optimum x-ray spectra for mammography *Phys. Med. Biol.* **27** 1209–20

Berns E A, Hendrick R E and Cutter G R 2003 Optimization of technique factors for a silicon diode array full-field digital mammography system and comparison to screen-film mammography with matched average glandular dose *Med. Phys.* **30** 334–40

Boone J M 1992 Parametrized x-ray absorption in diagnostic radiology from Monte Carlo calculations: implications for x-ray detector design *Med. Phys.* **19** 1467–73

Boone J M, Fewell T R and Jennings R J 1997 Molybdenum, rhodium, and tungsten anode spectral models using interpolating polynomials with application to mammography *Med. Phys.* **24** 1863–74

Boone J M, Lindfors K K, Cooper V N III and Seibert J A 2000 Scatter/primary in mammography: comprehensive results *Med. Phys.* **27** 2408–16

Caldwell C B and Yaffe M J 1990 Development of an anthropomorphic breast phantom *Med. Phys.* **17** 273–80

Calicchia A *et al* 1994 Molybdenum filter optimization in mammography *Physica Medica* **X** 55–60

Calicchia A, Gambaccini M, Indovina P L, Mazzei F and Pugliani L 1996 Niobium/molybdenum K-edge filtration in mammography: contrast and dose evaluation *Phys. Med. Biol.* **41** 1717–26

Cooper V N, Boone J M III, Seibert J A and Pellot-Barakat C J 2000 An edge spread technique for measurement of the scatter-to-primary ratio in mammography *Med. Phys.* **27** 845–53

Court L E and Speller R 1995 A multiparameter optimization of digital mammography *Phys. Med. Biol.* **40** 1841–61

Dobbins J T III *et al* 2003 Chest radiography: optimization of x-ray spectrum for cesium iodide-amorphous silicon flat-panel detector *Radiology* **226** 221–30

Dobbins J T III and Powell A O 1989 Variable compensation technique for digital radiography of the chest *Radiology* **173** 451–8

Fahrig R and Yaffe M J 1994a A model for optimization of spectral shape in digital mammography *Med. Phys.* **21** 1463–71

Fahrig R and Yaffe M J 1994b Optimization of spectral shape in digital mammography: dependence on anode material, breast thickness, and lesion type *Med. Phys.* **21** 1473–81

Goodsitt M M *et al* 1998 Classification of compressed breast shapes for the design of equalization filters in x-ray mammography *Med. Phys.* **25** 937–48

Huda W, Krol A, Jing Z and Boone J M 1998 Signal to noise ratio and radiation dose as function of photon energy in mammography *Proc. SPIE* **3336** 355–63

Huda W, Sajewicz A M, Ogden K M and Dance D R 2003 Experimental investigation of the dose and image quality characteristics of a digital mammography imaging system *Med. Phys.* **30** 442–8

Jennings R J, Eastgate R J, Siedband M P and Ergun D L 1981 Optimal x-ray spectra for screen-film mammography *Med. Phys.* **8** 629–39

Keshavmurthy S P, Goodsitt M M, Chan H P, Helvie M A and Christodoulou E 1999 Design and evaluation of an external filter technique for exposure equalization in mammography *Med. Phys.* **26** 1655–69

Kwok Leung L and Heang-Ping C 1990 Effects of x-ray beam equalization on mammographic imaging *Med. Phys.* **17** 242–9

LaVoy T R, Huda W and Ogden K M 2002 Radiographic techniques in screen-film mammography *J. Appl. Clin. Med. Phys.* **3** 248–54

Maidment A D, Fahrig R and Yaffe M J 1993 Dynamic range requirements in digital mammography *Med. Phys.* **20** 1621–33

Molloi S, Tang J, Mather T and Zhou Y 1999 Area x-ray beam equalization for digital angiography *Med. Phys.* **26** 2684–92

Molloi S, Van Drie A and Wang F 2001 X-ray beam equalization: feasibility and performance of an automated prototype system in a phantom and swine *Radiology* **221** 668–75

Molloi S, Zhou Y and Wamsely G 1998 Scatter-glare estimation for digital radiographic systems: comparison of digital filtration and sampling techniques *IEEE Trans. Med. Imaging* **17** 881–8

Molloi S Y and Mistretta C A 1988 Scatter-glare corrections in quantitative dual-energy fluoroscopy *Med. Phys.* **15** 289–97

Motz J W and Danos M 1978 Image information content and patient exposure *Med. Phys.* **5** 8–22

Muller S 1999 Full-field digital mammography designed as a complete system *Eur. J. Radiol.* **31** 25–34

Muntz E P, Jafroudi H, Jennings R and Bernstein H 1985 An approach to specifying a minimum dose system for mammography using multiparameter optimization techniques *Med. Phys.* **12** 5–12

Ogden K M, Huda W and Scalzetti E M 2003 A general approach to optimizing digital mammography with respect to radiation risk *Proc. SPIE* **5030** 908–14

Panayiotakis G *et al* 1998 Evaluation of an anatomical filter-based exposure equalization technique in mammography *Br. J. Radiol.* **71** 1049–57

Sabol J M and Plewes D B 1996 Analytical description of the high and low contrast behavior of a scan-rotate geometry for equalization mammography *Med. Phys.* **23** 887–98

Sabol J M, Soutar I C and Plewes D B 1993a Mammographic scanning equalization radiography *Med. Phys.* **20** 1505–15

Sabol J M, Soutar I C and Plewes D B 1993b Observer performance and dose efficiency of mammographic scanning equalization radiography *Med. Phys.* **20** 1517–25

Sabol J M, Soutar I C and Plewes D B 1996 Practical application of a scan-rotate equalization geometry to mammography *Med. Phys.* **23** 1987–96

Sobol W T and Wu X 1997 Parametrization of mammography normalized average glandular dose tables *Med. Phys.* **24** 547–54

Tesic M M, Piccaro M F and Munier B 1997 Full field digital mammography scanner *Eur. J. Radiol.* **31** 2–17

Wu X, Barnes G T and Tucker D M 1991 Spectral dependence of glandular tissue dose in screen-film mammography *Radiology* **179** 143–8

Xu T *et al* 2004 Area beam equalization: optimization and performance of an automated prototype system for chest radiography *Acad. Radiol.* **11** 377–89

Zamenhof R G 1982 The optimization of signal detectability in digital fluoroscopy *Med. Phys.* **9** 688–94